HHS Public Access

Author manuscript

Nat Struct Mol Biol. Author manuscript; available in PMC 2014 November 01.

Published in final edited form as:

Nat Struct Mol Biol. 2014 May ; 21(5): 472–479. doi:10.1038/nsmb.2816.

Conformational dynamics of ligand-dependent alternating access in LeuT

Kelli Kazmier[1], **Shruti Sharma**[2], **Matthias Quick**[3,4,5], **Shahidul M. Islam**[6], **Benoit Roux**[6], **Harel Weinstein**[7,8], **Jonathan A. Javitch**[3,4,5,9], and **Hassane S. Mchaourab**[1,2]

[1]Chemical and Physical Biology Program, Vanderbilt University Nashville, Tennessee, USA

[2]Department of Molecular Physiology and Biophysics, Nashville, Tennessee, USA

[3]Center for Molecular Recognition, Columbia University College of Physicians and Surgeons, New York, New York, USA

[4]Department of Psychiatry, Columbia University College of Physicians and Surgeons, New York, New York, USA

[5]New York State Psychiatric Institute, Division of Molecular Therapeutics, New York, New York, USA

[6]Department of Biochemistry and Molecular Biology, University of Chicago, Chicago, Illinois, USA

[7]Department of Physiology and Biophysics, Weill Medical College of Cornell University, New York, New York, USA

[8]HRH Prince Alwaleed Bin Talal Bin Abdulaziz Alsaud Institute for Computational Biomedicine, Weill Medical College of Cornell University, New York, New York, USA

[9]Department of Pharmacology, Columbia University College of Physicians and Surgeons, New York, New York, USA

Abstract

The leucine transporter (LeuT) from *Aquifex aeolicus* is a bacterial homolog of neurotransmitter:sodium symporters (NSS) that catalyze reuptake of neurotransmitters at the synapse. Crystal structures of wild type (WT) and mutants of LeuT have been interpreted as conformational states in the coupled transport cycle. However, the mechanistic identities inferred from these structures have not been validated and the ligand-dependent conformational equilibrium of LeuT has not been defined. Here, we utilized distance measurements between spin label pairs to elucidate Na^+- and leucine-dependent conformational changes on the intracellular

All correspondence should be addressed to H.S.Mhassane.mchaourab@vanderbilt.edu.
K.K. and S.S. contributed equally to this manuscript.

Author Contributions

K.K. and S.S. constructed mutants, expressed and purified protein, prepared samples and conducted DEER experiments. K.K. and H.S.M. designed the DEER experiments. K.K., S.S. and H.S.M. analyzed DEER data and interpreted the distance distributions. M.Q. designed, conducted, and analyzed Leu binding and Ala transport experiments. S.M.I. and B.R. refined structural models using the restrained ensemble simulations method. All authors contributed to the mechanistic interpretation of the data, wrote, and edited the manuscript.

and extracellular sides of the transporter. The results identify structural motifs that underlie the isomerization of LeuT between outward-facing, inward-facing and occluded states. The novel conformational changes reported here present a dynamic picture of the alternating access mechanism of LeuT and NSS that is different to the inferences reached from currently available crystal structures.

Introduction

Neurotransmitter:sodium symporters (NSS) include biogenic amine transporters that terminate synaptic signaling through selective reuptake of neurotransmitter molecules[1]. As targets of antidepressant molecules[2] and drugs of abuse[3], these transporters are critical in a spectrum of neuropsychiatric disorders[4,5] and in substance addiction disorders[5]. The leucine transporter (LeuT) is a bacterial Na^+-coupled amino acid transporter from *Aquifex aeolicus* with broad specificity for small hydrophobic amino acids[6,7]. It has emerged as a paradigm for NSS transporters owing to sequence, structural and functional similarities that extend from highly conserved residues involved in ion and substrate coordination[6,8,9] to an overlapping spectrum of transport inhibitors[10]. LeuT is also the founding member of a fold class that encompasses sequence-unrelated symporters and antiporters. The conserved motif consists of an inverted repeat[11] of two sets of five transmembrane helices that coordinate the ions and substrates bound in a site near the middle of the membrane, which is often stabilized by electrostatic interactions with unwound regions of transmembrane helices (TM) 1 and 6 (ref. 6).

The current dogma of secondary active transport postulates “alternating access” of the transporter that requires transition between at least two conformational states in which the ion and substrate binding sites are alternately exposed to the two sides of the membrane[12–15]. In this context, crystal structures of representative LeuT-fold transporters from multiple superfamilies have been classified as inward-facing, outward-facing or substrate-occluded states, cast as intermediates in the transport cycle, and then interpolated to infer plausible pathways of substrate binding and release[16–20]. A model of LeuT alternating access has emerged from crystal structures in three conformations (PDB ID: 3TT1[16], PDB ID: 3TT3[16], PDB ID: 2A65[6] (Fig. 1)). Mutation of highly conserved residues and subsequent conformational selection by antibodies were used to capture the inward- and outward-facing states[16]. However, the inference that the structures of these mutants represent actual intermediates in the alternating access cycle has not been verified. Molecular dynamics (MD) simulations[21,22] and homology modeling[11] have elaborated specific structural models of LeuT alternating access. A rocking bundle model[11,23] envisioned conserved rearrangements between rigid scaffold and bundle domains in switching between outward- and inward-facing conformations. Steered MD simulations of LeuT uncovered a second substrate binding site that was proposed to allosterically control the opening of an intracellular gate[21]. However, despite the wealth of structural data and extensive computational analyses, there is no consensus on the suite of conformational states that underlie alternating access in LeuT-fold transporters. A critical step towards this goal is the validation of the mechanistic identities of the available crystal structures and their incorporation into a dynamic framework of ion- and substrate-dependent equilibria[24–26].

Here, we utilized Site-Directed Spin-Labeling (SDSL)[27] and Double Electron-Electron Resonance (DEER) spectroscopy[28] to measure distance probabilities between spin label pairs in LeuT in order to (i)– define the ligand-dependent conformational equilibrium of LeuT, (ii)– identify the structural elements that mediate alternating access, and (iii)– investigate whether the LeuT conformational cycle involves isomerization between the structures identified in the crystal. From the interpretation of these results emerges a new model for the mechanism of LeuT alternating access that is at variance with the current picture inferred from the crystal structures[16].

Results

To define the ligand-dependent equilibrium of LeuT between conformational states, we measured distance distributions between spin label pairs under ligand conditions expected to promote transitions between transport intermediates[29,30]. An extensive set of spin label pairs was designed to report a comprehensive view of the extracellular and intracellular sides of the transporter. On the extracellular side, distances were referenced to two sites in TMs 3 and 5 expected to be static. On the intracellular side, reference sites were selected in TMs 4 and 9.

We verified that all spin-labeled LeuT mutants introduced in the WT background bind leucine (Supplementary Fig. 1) in a Na^+-dependent manner. We observed changes in the level of binding relative to WT (dashed line, Supplementary Fig. 1a) for mutants in TM6 as well as for spin label pairs introduced in a Y268A background or an R5A background (red bar graph, Supplementary Fig. 1a). These two background mutations were constructed to mimic the disruption of an intracellular hydrogen bonding network[29,31], as observed in the inward-facing LeuT crystal structure[6]. Analysis of binding isotherms demonstrates that the lower level of binding reflects lower affinity, but similar substrate stoichiometry relative to the WT (Supplementary Fig. 1b). In addition, we measured Na^+-dependent alanine uptake in proteoliposomes for a large subset of mutants that are central to the interpretation of the results presented in this paper (Supplementary Fig. 2a,b). These data confirm that cysteine substitution and spin labeling do not impair the transport function of LeuT, consistent with the findings from binding measurements.

LeuT Na^+ and Leu-dependent conformational equilibrium

DEER distance distributions describe the distance probabilities between a pair of spin labels[27,28]. In addition to reporting the average distance, the width of these distance distributions reflects dynamic modes that modulate the distance between the two spin labels[24,32,33]. Conformational sampling at room temperature is manifested as static disorder in the solid state conditions under which the DEER data are collected. Thus, the broad and multi-component distance distributions between pairs of labeled residues on the extracellular side of LeuT (Fig. 2a–d) are consistent with fluctuations between multiple conformations at equilibrium. To facilitate the assignment of distance components, we used different ligand conditions to enhance the populations of transporters in particular conformations. In the presence of Na^+ and Leu (red traces, Fig. 2), the distribution would be expected to favor the state captured by the crystal structure of Na^+- and Leu-bound LeuT (PDB ID: 2A65)

classified as substrate-occluded[6]. In the presence of Na^+ (blue traces, Fig. 2), the transporter would be expected to favor an outward-facing conformation poised to bind substrate[21,30]. In the absence of ion and substrate (apo condition), LeuT is expected to sample inward-facing, outward-facing, and occluded conformations.

Our analysis identified two structural motifs, one consisting of extracellular loop (EL) 4 and TM6a (Fig. 2a,b), and the other consisting of TMs 1b and 7b (Fig. 2c,d). The first motif responded to Na^+ binding by an "outward-opening" that increased the population of the longer component in the distance distributions relative to apo (Fig. 2a,b). This component represents conformation(s) wherein TM6a moves away from reference points in TMs 3 and 5 while EL4 moves away from EL6. Notably, the second motif was relatively less sensitive to Na^+, suggesting that even under apo conditions it already favored an outward-open conformation (Fig. 2c,d). As previously reported[30], transition to an outward-open conformation involves movements of extracellular loops, including EL2, EL3 and EL4, and is accompanied by increased water accessibility in the permeation pathway that leads to the binding site. Thus, we conclude that the movement of the two motifs underlies the change in accessibility of this vestibule.

We found that leucine binding induced concurrent shifts in the distance distributions of TMs 1, 6, and 7 and EL4 to favor the component associated with their closed positions (red traces, Fig. 2). In this presumably substrate-occluded conformation, TMs 1b, 6a and 7b moved closer to reference points in TMs 3 and 5. We infer that this movement is reponsible for the reported reduced water accessibility in the vestibule upon leucine binding[30]. For TMs 1b, 6a, 7b, and EL4, the magnitude of changes in the average distance between components corresponding to the outward-facing and substrate-occluded conformations was consistently >5Å larger than that predicted by comparing crystal structures of the states defined as outward-facing and substrate-occluded states (Fig. 1a, ribbon scale) (see below).

Similar interrogation of the dynamics at the intracellular side with a network of spin label pairs identified TMs 6b and 7a and the N-terminal segment as undergoing the most substantial Na^+ and Leu-dependent movements (Fig. 3a–d). TM7a distance distributions were distinctly bimodal in the apo conditions, reflecting the equilibrium between inward-open and inward-closed conformations (Fig. 3b). The distances between TM7 and reference points in TM4 and IL1 decreased with inward-opening. Na^+ and Na^+ and Leu binding shifted the equilibrium in the same direction, *i.e.* favored the same distance component, consistent with both conditions stabilizing an inward-closed conformation (blue and red traces, Fig. 3b). The nature of the TM6b movement was more challenging to define because its buried environment hindered spin label incorporation at non-destabilizing, exposed sites (Supplementary Figs. 1, 2, and 3). Nevertheless, spin label pairs monitoring distances between the C-terminal loop of TM6 (intracellular loop (IL) 3) and TM4 showed ligand-dependent changes in average distance and distribution width (Fig. 3a). The N-terminal segment (residues 1–10) displayed a Na^+- and Leu-dependent shift between two populations that represent the transition between the inward-open (longer distance component) and the inward-closed positions (shorter distance component) (Fig. 3c). Presumably, this movement is associated with release of a putative intracellular gate consisting of a network of charge

interactions involving the N-terminus and IL1 and stabilized by Tyr268 in IL3[31] (Supplementary Fig. 3a).

Distance changes identify novel LeuT conformational changes

On the basis of the inward-facing crystal structure[16], a large displacement of TM1a away from TM3 and TM9 that lifts it upward towards the middle of the membrane is expected, along with a sizeable translation of TM5 relative to a scaffold of helices (Fig. 1b, ribbon scale). Surprisingly, TM1a distance distributions measured here did not show components that would correspond to such a large amplitude movement (Fig. 3c), although changes in distribution widths indicated small scale adjustments of TM1's position relative to TMs 3 and 9. Furthermore, TM5 distributions were consistently narrow and the relative distance to other helices did not change as a result of Na^+ or Na^+ and Leu binding (Fig. 3d).

To characterize and quantify the discrepancies between our DEER results and the inferences based on the crystal structures, we compared distance distributions measured here with the distance distributions expected in the various crystals structures, the latter determined using the benchmarked spin label rotamer library MMM[34,35] (Supplementary Figs. 4 and 5). On the extracellular side, a pattern of inconsistencies emerged in the distributions between TMs 1 or 6, and TMs 3 and 5 (Supplementary Fig. 4). Specifically, the distance component assigned to the occluded conformation (*i.e.* solid red trace favored by Na^+ and Leu, Fig. 2b,c) was consistently shorter than any component in the predicted distributions based on the 2A65 structure (Supplementary Fig. 4). Thus, we infer that this crystal structure underestimates the closing of TMs 1b and 6a induced by Na^+ and Leu binding in solution. Furthermore, the predicted distributions between TM7 and TMs 3 and 5 in the crystal structures of outward-open[16] and substrate-occluded[6] states (Fig. 1a, ribbon scale) are superimposable, which is inconsistent with the prominent movement of TM7b, implied by the change in the distance distribution we observed in the presence of Na^+/Leu (Fig. 2d). Finally, while comparison of these crystal structures suggests movements of TM2 relative to TMs 3 and 5, we observed a tight distribution for these distances that is similar in the apo, Na^+-bound and Na^+- and Leu-bound conditions (Supplementary Fig. 4).

β-OG may select for an outward-facing conformation

We reasoned that β-octyl glucoside (β-OG), the detergent used in most crystallization conditions[6,16] might be responsible for the discrepancies between our measurements of extracellular occlusion and those predicted by the crystal structures (Fig. 4a–d). Indeed, we found that exchange of LeuT from β-dodecyl maltoside (β-DDM) into β-OG shifts the experimental distance distributions for TMs 1, 2, 6 and 7 (Fig. 4b) towards the distance component assigned to the outward-open conformation (red arrows, Fig. 4c), thereby partly or fully resolving the quantitative discrepancy with predicted distributions (Fig. 4d). This is consistent with the notion that a more outward-open conformation is favored in β-OG even in the presence of Na^+ and Leu, presumably as a result of the binding of a β-OG molecule in the extracellular vestibule (Fig. 4a)[36]. Together, these findings are consistent with 2A65 representing an outward-facing state and not an occluded configuration that we observe in solution and is expected upon Na^+/Leu binding.

On the intracellular side, the components in the distance distributions corresponding to the Na^+ and Leu state for TMs 1 and 2 tended to be larger than those predicted from the substrate-occluded structure (2A65)[6] (Supplementary Fig. 5). The direction of the deviation and the effects of Na^+ and Leu suggest that TM1 favors a more open conformation relative to that observed in the outward-facing[16] or substrate-bound[6] crystal structures. In contrast to the extracellular side, the shift in the distance distributions upon exchange into β-OG favored the shorter distance component (red arrows, Fig. 4b,c), which overlapped with the distribution predicted based on the occluded crystal structure determined in the presence of Na^+ and Leu (Fig. 4d). Thus the LeuT conformation in β-OG is more outward-open/inward-closed, both in the 2A65 structure and in our DEER measurements. This suggests that the actual substrate-occluded state (in the absence of β-OG) is more closed at the extracellular side and more open at the intracellular side than the 2A65 structure.

Y268A mutation uncouples helical movements from Na^+ and Leu binding

Crystallization of LeuT in the inward-open structure required multiple mutations to disrupt the intracellular gate and to weaken the Na2 site[16]. The former was achieved through the substitution of a highly conserved tyrosine (Tyr268) in TM6b with an alanine. Therefore, we monitored the distance distributions of TM1a and TM5 on the intracellular side in a Y268A background (Fig. 5a–c). Compared to distance distributions in the WT background (Fig. 5b), the pattern of distance changes in this mutant background (Fig. 5c) recapitulated many aspects of the inward-facing[16] crystal structure (Fig. 5a). TM1 underwent a 15 Å change in distance relative to TM9 (dashed lines, Fig. 5c), which lifted it towards the middle of the membrane leading to a short distance component relative to the extracellular side of TM8 (Supplementary Fig. 6). The marked displacement of TM5 deduced from the inward-facing crystal structure (Fig. 5a) was also captured by the distance distribution to TM9 (Fig. 5b,c). However, this “opening” movement of TM5 was not reversed by the presence of Na^+ and Leu (Fig. 5c, red dashed traces), despite direct biochemical evidence that these mutants bind Leu, albeit with lower affinity (Supplementary Figs. 1, 2). Thus, in the mutant background, TM5 did not reset to its closed position even in the presence of Na^+ and Leu. Another mutation that was shown to disrupt the intracellular gate, R5A (Fig. 5a, Supplementary Fig. 3a)[29,31], yielded distance changes similar to Y268A (Fig. 5c). Thus, the mutations used to generate the inward-open[16] crystal structure shift a major population of the transporters to a conformation that is not readily observed in the ensemble of states sampled in the WT background.

Restrained ensemble modeling of LeuT conformational changes

To describe the coordinated structural changes induced by Na^+ and Leu binding, we carried out MD simulations restrained by the DEER distance distributions using the recently described restrained ensemble (RE) method[37,38]. Multiple copies of “dummy” spin labels, previously parameterized from all-atom simulations of the spin-label, were inserted at sites for which the DEER distance distribution data are available (Fig. 6a–f) and the transporter backbone was allowed to adjust dynamically to match the experimental distributions. The experimental distance distributions were effectively imposed to the multiple copies of the dummy spin labels via a large harmonic potential (see methods). For all the simulations, the substrate-occluded crystal structure (2A65) was used as the starting conformation. TMs 2–5,

8 and 9 were held fixed on the basis of distance distributions that did not change in response to ligand binding (Supplemental Figure 7). We found that imposing the DEER restraints corresponding to the Na^+-bound state did not lead to substancial changes in the LeuT structure, consistent with our finding that it represents an outward-facing conformation (Fig. 6a–c). In contrast, substantial changes in the backbone were observed when the structure was refined using DEER restraints from the Na^+- and Leu-bound state, with notable shifts of extracellular TMs 1 and 6 towards the vestibule as expected from a closing motion (Fig. 6a–c). The movement of extracellular TM7 was in a different direction, but we suggest that this motion enabled the capping of the vestibule by EL4[30]. Similarly, we found that imposing the EPR restraints representing the inward-facing conformation drove backbone changes in the N-terminus, TMs 1 and 7 on the intracellular side (Fig. 6d–f). However, the amplitudes of these changes were smaller than those demonstrated experimentally in the distance distributions. In this case, the backbone displacements have been largely obscured by excessive rotameric sampling of the dummy label, which was previously optimized to best match DEER data for solvent-exposed sites in T4 Lysozyme but which might be over-estimated in the present situation[37,38]. This effect was also present on the extracellular side, limiting the magnitude of evident conformational changes, but to a lesser degree. A contributing factor to this discepancy may have been the sparsity of restraints on the intracellular side, limited by design as a consequence of tight packing of secondary structures. Overall, the RE simulations confirm that the Na^+ and Na^+-Leu bound crystal structures represent outward-facing structures, demonstrate that the inward-facing crystal structure is incompatible with the DEER data in the WT background, and outline the structural elements involved in the transition to the occluded and inward-facing conformations, neither of which was observed previously[6,16].

Discussion

Structural motifs underlying alternating access of LeuT

The pattern and ligand dependence of distance changes gleaned from the distributions and validated by the RE simulations identifies movements of motifs at the extracellular (1b/7b and 6a/EL4) and intracellular ends (6b/7a, N-term) of LeuT (Fig. 7). In the absence of ligands, both motifs can sample open and closed positions enabling apo-LeuT to isomerize between conformations, as would be expected for a symporter (Fig. 7a,f), although the equilibrium favors the inward-facing conformation. Binding of Na^+, which engages the unwound segments of TMs 1 and 6, concomitantly shifts the equilibria of the extracellular and intracellular motifs, effectively favoring an outward-open/inward-closed conformation of LeuT (Fig. 7b). Substrate, which is primarily coordinated by the unwound regions of TMs 1 and 6 in the primary binding site (S1), resets these two TMs to their closed positions (Fig. 7c). Together, these observations suggest that the rearrangements of the intracellular and extracellular motifs reported here are mechanistically important for the alternating access mechanism in LeuT.

One of the major findings of this work is that the ligand-dependent coupling of the extracellular side of the transporter with its intracellular side involves both TMs 6 and 7. While TM6 was proposed to be a pivotal element in the isomerization of LeuT based on its

direct contact with ligands, the ion- and substrate-dependent movement of TM7 described here is novel. The coupled but opposite shifts in the equilibria of the extracellular part of TM6 (TM6a) and the intracellular part of TM7 (TM7a) ensure that the intracellular motif and the extracellular motifs are not concurrently open. We suggest that the movement of TM7 was obscured in the crystal structures by the tendency to trap LeuT in outward-facing conformations, possibly by the binding of β-OG in the extracellular vestibule[6,16].

The proposed movement of the intracellular and extracellular motifs are grounded in aspects of TM flexibility that have been inferred from the crystal structures[6,16]. Specifically, the pivot points observed crystallographically in TMs 1, 6, and 7 rationalize the hinge-like bending of these TMs required for the transition between inward-facing and outward-facing states in our model (Fig. 7). Although TM7 does not have an unwound region, a hinge-like bend at Gly294 was evident in the inward-facing crystal structure. Small ion/substrate-dependent movements are noted for TMs 1, 10 and 11 on the intracellular side; the latter two most likely serve to facilitate the movement of the intracellular motif that they cradle (Supplementary Fig. 7b). Importantly TM1a's more open position relative to the crystal structure (see Figure 4) is consistent with MD simulations[22] that invoke TM1 movement in facilitating substrate release. Notably, these simulations were initiated from the Na^+ and Leu crystal structure, so that the dynamic nature of TM1 in the simulations may reflect both the relaxation to its position in the occluded conformation in the absence of β-OG and the response to the progress of substrate towards the intracellular release site. Indeed, the broad distributions of TM1 suggest that this helix is relatively dynamic, and with TM1a favoring a more open position relative to the 2A65 structure, the movement of the intracellular motif (Fig. 7d–f) enables substrate exit on the intracellular side of the transporter. Krishnamurthy et al. proposed[16] that in the absence of bound Na^+, it is energetically unfavorable for TM1 to remain in a "closed" position. While our data support a dynamic TM1 under apo conditions, the implication that it is favorable for TM1 to lift up into the membrane now seems unlikely given the absence of large amplitude, ion-dependent movement of this TM in the WT background.

Mechanism of transport

Coupled transport requires the binding of ions and substrates on one side of the membrane, followed by conformational changes to enable subsequent ion and substrate dissociation at the other side of the membrane. Symported ions that power the uphill movement of substrates, could stabilize and destabilize substrate binding in the outward- and inward-facing conformations, respectively, conferring directionality to the transport process by their concentration gradients. Additionally, ion binding could alter the energetics of the equilibrium in the ensemble of conformations, increasing the population of those conformations where the substrate site is open to the extracellular milieu. In LeuT, Na^+ fulfills both roles: its binding biases the equilibrium to favor an outward-facing conformation and it subsequently directly coordinates the substrate at the unwound regions of TMs 1 and 6.

We and others[29,30] find that substrate binding induces occlusion of the binding site on both sides of the transporter (Fig. 7c). Thus, the energetically unfavorable release of Leu, has to

be facilitated by low probability equilibrium fluctuations of the intracellular motif (TMs, 6, 7 and N-terminus) to its open position (Fig. 7d). We surmise that these fluctuations must be coupled to the favorable movement of Na^+ down its concentration gradient. Previous studies[21,39] proposed that the dissociation of Na^+ at Na2 (Fig. 7e) in the presence of substrate in both the primary binding site (S1) and a secondary binding site (S2) enhances inward opening and facilitates inward release of the Na^+ at Na1. The loss of this Na^+ reduces the affinity of substrate, which enhances its dissociation to the cytoplasm (Fig. 7f). Furthermore, it was implied[39] that fluctuations of the intracellular motif to its open position could be enhanced by the binding of substrate at S2, which is located in the extracellular vestibule in contact with the tip of EL4[21]. A plausible mechanism for allosteric regulation by substrate binding at S2 would involve structural rearrangements initiated at EL4 and propagated by TM7a and b, culminating in repositioning TM6b in an inward-open position (Fig. 7c–e).

The transport cycle scheme presented in Figure 7 departs from the rocking bundle model[11,23] in fundamental aspects. The latter invokes rotation of the entire bundle relative to the scaffold to mediate the alternating access of the transporter. Although TMs 1, 6 and 7 are part of the bundle, they do not move as rigid bodies but flex around hinge points. Moreover, the extracellular and intracellular opening and closing are not mediated by the same helices. Notably TM2's movement does not substantially change its distance relative to the scaffold in response to ligand binding. Finally, the prominent movement of EL4 and the N-terminal region, are not considered in the rocking bundle model.

The new insight offered by the data presented here suggests a novel set of conformational changes underlying alternating access by LeuT, and set the stage for further analysis to determine the transition path between these states. This is a critical step towards elucidating the mechanism of Na^+-coupled transport by LeuT and LeuT-fold transporters.

Methods

Mutagenesis, expression, purification and labeling of LeuT

All LeuT mutations were introduced into the recombinant LeuT construct containing an N-terminal decahistidine tag[21] using PCR-based site-directed mutagenesis and confirmed by DNA sequencing. Mutant LeuT was expressed in *Escherichia coli* BL21(DE3) as previously described[21]. LeuT was washed three times in 200mM Tris-MES, pH 7.5, 20% (v/v) glycerol to remove bound leucine and subsequently extracted from native membranes with 40 mM (2% w/v) *n*-dodecyl-β-maltoside (β-DDM, Anatrace). LeuT was purified by Ni^{2+} affinity chromatography and spin-labeled with 0.35 mM *S*-(2,2,5,5-tetramethyl-2,5-dihydro-1H-pyrrol-3-yl)methyl methanethiosulfonate spin label (MTSSL, Enzo Life Sciences) for 2 hours at room temperature and 4 °C overnight. Spin labeled LeuT was separated from free spin labels and aggregated protein using size exclusion chromatography performed on a Shodex KW-803 column in a buffer consisting of 200 mM Tris-MES buffer, 0.05% (w/v) β-DDM and 20% (v/v) glycerol at pH 7.2. LeuT was concentrated with Amicon Ultra columns (100 kDa, Millipore). For *n*-octyl-β-D-glucoside (β-OG, Anatrace) samples, Na^+ and excess Leu were added to Ni-affinity purified LeuT, the mixture purified by size exclusion chromatography in β-OG buffer (200 mM Tris-MES pH7.2, 200 mM NaCl, 1 M leucine,

20% glycerol (v/v), 40 mM (1.2% w/v) β-OG), and subsequently concentrated with Amicon Ultra columns (50 kDa, Millipore). Protein concentration was determined using an extinction coefficient of 1.91 cm^{-1} mg^{-1} at 280 nm for all mutants. All DEER samples were prepared in the 50 – 200 M protein concentration range. A final concentration of glycerol of 30% (w/v) was used in all samples as a cryoprotectant. The Na^+ state was obtained by addition of 200 mM NaCl. The Na^+ and Leu state was obtained by adding 4 times molar excess of Leu to protein, in addition to 200 mM NaCl.

LeuT functional analysis

Equilibrium binding of ^{3}H-leucine (140 Ci/mmol; American Radiolabeled Chemicals, Inc.) at the indicated concentrations and specific radioactivities was performed with the scintillation proximity assay (SPA)[40]. 0.8 pmol of unconcentrated purified and spin-labeled LeuT were bound to 250 μg copper-coated YSi-SPA beads (Perkin Elmer) in 100 μL assay buffer (150 mM Tris-Mes, pH 7.5, 50 mM NaCl, 1 mM TCEP, 20% (v/v) glycerol, 0.1% (w/v) β-DDM) for 16 h at 4 °C prior to measuring the samples in a Wallac photomultiplier tube MicroBeta ™ microplate counter in the SPA mode. To determine the non-proximity background signal, samples were incubated in the presence of 800 mM imidazole, which competes with the His-tagged protein for binding to the copper-coated SPA beads. The non-proximity signal (in counts per minute, cpm), was subtracted from the total cpm (in the absence of imidazole) to obtain the specific cpm. Data points show the mean ± the SEM of triplicate determinations normalized as a percentage of WT. Experiments were conducted using 100, 1000, or 1500 nM ^{3}H-leucine. Saturation binding curves were constructed for a subset of representative LeuT mutants by varying ^{3}H-leucine concentration between 10 nM and 5 M and are normalized as a percentage of WT. Curves were fitted using the non-linear curve fit, one site binding function in Origin 8 (OriginLab).

Transport assays of reconstituted LeuT variants were performed as described[21,40]. Briefly, purified LeuT variants were reconstituted at a 1:150 (w/w) ratio in preformed liposomes made of *E. coli* polar lipid extract (Avanti). 1 M [^{3}H]-Ala (49.4 Ci/mmol, Moravek) transport was measured for the indicated periods of time at 22 °C in assay buffer composed of 50 mM Tris-Mes, pH 8.5, 50 mM NaCl and stopped by quenching the samples with ice cold 100 mM Kpi, pH 6.0, 100 mM LiCl followed by rapid filtration through 0.22 μm nitrocellulose filters (Millipore) and scintillation counting. Cpm were transformed into mol using known amounts of ^{3}H-Ala.

DEER spectroscopy

Distance measurements were conducted on a Bruker 580 pulsed electron paramagnetic resonance (EPR) spectrometer operating at Q-band frequency (33.9 GHz) using a standard four-pulse DEER sequence as previously described[41]. All DEER experiments were performed at 83 K. The frequency difference between pump and observed was typically 63 MHz. Dipolar evolution times were designed to allow identification of background slopes, when possible. Echo decays were shortened by 500 ns to remove the baseline step that results from overlap between pump and observe pulse as previously described[42]. background-corrected and fit with the DEER Analysis 2011 program[43] using Tikhonov regularization[44] to obtain distance distributions. Aggregated protein, resulting from

concentration and validated by gel electrophoresis, appears in some samples as a non-specific distribution peak near 50 Å. This peak shifts depending on the decay time of the echo suggesting a broad distribution. This assignment was confirmed by re-analysis of the sample following DEER measurements by size-exclusion chormatography.

Rotamer simulation

Distance distributions for each mutant were simulated for LeuT crystal structures (PDB ID: 2A65, 3TT1, 3TT3) using the rotamer library-based prediction software MMM 2011 (refs. 34, 35). Rotamer library calculations were conducted at 83K.

Restrained ensemble simulations

The restrained ensemble (RE) simulation method[37,38] was used to model LeuT conformations using the DEER distance distribution data. The crystal structure of the Na^+ and Leu occluded state (2A65)[6] was used to construct the initial geometry for the simulations. All simulations were carried out with the CHARMM[45] program modified to account for the DEER distance histogram restraints via the RE simulation method. The all-atom CHARMM27 protein force field[46] with the CMAP corrections[47] was used. The dummy nitroxide spin label was parameterized and optimized previously from all-atom simulations of the MTSSL spin-label to best-match DEER data on several solvent-exposed sites in T4 Lysozyme[37]. The EEF1 and IMM1 implicit membrane model[48,49] was used to mimic the bilayer membrane environment and was centered at Z = 0 with the membrane-normal parallel to the Z axis. The EEF1 and IMM1 calculations were prepared using the Implicit Solvent Modeler module in CHARMM-GUI (www.charmm-gui.org)[50]. The simulations were performed under NVT conditions at 300 K and the Langevin[51] thermostat was used to control the temperature of the simulation box. A collision frequency, γ, of 1 ps^{-1} was used for the Langevin thermostat and an integration time step of 1 fs was employed. The nonbonded interactions were smoothly switched off from 7–11Å using a group-based cutoff. The mutiple copies of the dummy spin labels were initially optimized using energy minimization, and then replicated 25 times to yield a total of 625 distances between each spin-label pair for constructing the histograms. After a weakly restrained (10 kcal/mol·$Å^2$) 25 ps system equilibration, the RE simulation used root-mean-square deviation (RMSD) restraints (500 kcal/mol·$Å^2$) to maintain secondary structure in helical residues, positional harmonic restraints on residues 41–214 and 337–395 to maintain crystal structure positions for static regions, and distance distribution restraints to drive conformational change in dynamic regions. Distance distribution data corresponding to apo, Na^+-bound, and Na^+- and Leu-bound intermediates were used for three different RE simulations. Each RE simulation was performed for 10 ns, which for each simulation was past the time required for RMSD convergence to a constant value. An energy restraint was imposed via a large force constant (80000 kcal/mol) in order to match the calculated spin-pair distance distributions with those of the experiment with set to 1.7. The final structures thus obtained from the three RE simulations were then used for comparative analysis.

Supplementary Material

Refer to Web version on PubMed Central for supplementary material.

Acknowledgements

The authors gratefully acknowledge R. Stein for assistance with EPR data collection and EPR distance analysis. We thank H. Koteiche and P.R. Steed for critical reading and editing of the manuscript. We thank XSEDE for computer time. This work was supported by US National Institutes of Health grants U54-GM087519 (H.S.M., B.R., H.A.W., J.A.J., S.M.I., B.R.), K05DA022414 (J.A.J.) and P01DA012408 (H.A.W.). K.K. was supported by a predoctoral National Research Service Award (F31-MH095383-01).

References

1. Rudnick, G. Mechanisms of Biogenic Amine Neurotransmitter Transporters. In: Reith, MA., editor. Neurotransmitter Transporters. Humana Press; 2002. p. 25-52.
2. Iversen L. Neurotransmitter transporters and their impact on the development of psychopharmacology. Br J Pharmacol. 2006; 147(Suppl 1):S82–S88. [PubMed: 16402124]
3. Amara SG, Sonders MS. Neurotransmitter transporters as molecular targets for addictive drugs. Drug Alcohol Depend. 1998; 51:87–96. [PubMed: 9716932]
4. Singh SK. LeuT: A prokaryotic stepping stone on the way to a eukaryotic neurotransmitter transporter structure. Channels (Austin). 2008; 2
5. Gether U, Andersen PH, Larsson OM, Schousboe A. Neurotransmitter transporters: molecular function of important drug targets. Trends Pharmacol Sci. 2006; 27:375–383. [PubMed: 16762425]
6. Yamashita A, Singh SK, Kawate T, Jin Y, Gouaux E. Crystal structure of a bacterial homologue of Na+/Cl--dependent neurotransmitter transporters. Nature. 2005; 437:215–223. [PubMed: 16041361]
7. Singh SK, Piscitelli CL, Yamashita A, Gouaux E. A Competitive Inhibitor Traps LeuT in an Open-to-Out Conformation. Science. 2008; 322:1655–1661. [PubMed: 19074341]
8. Beuming T, Shi L, Javitch JA, Weinstein H. A Comprehensive Structure-Based Alignment of Prokaryotic and Eukaryotic Neurotransmitter/Na+ Symporters (NSS) Aids in the Use of the LeuT Structure to Probe NSS Structure and Function. Molecular Pharmacology. 2006; 70:1630–1642. [PubMed: 16880288]
9. Kanner BI, Zomot E. Sodium-Coupled Neurotransmitter Transporters. Chemical Reviews. 2008; 108:1654–1668. [PubMed: 18393466]
10. Kristensen AS, et al. SLC6 Neurotransmitter Transporters: Structure, Function, and Regulation. Pharmacological Reviews. 2011; 63:585–640. [PubMed: 21752877]
11. Forrest LR, et al. Mechanism for alternating access in neurotransmitter transporters. Proc Natl Acad Sci U S A. 2008; 105:10338–10343. [PubMed: 18647834]
12. Mitchell P. A general theory of membrane transport from studies of bacteria. Nature. 1957; 180:134–136. [PubMed: 13451664]
13. Jardetzky O. Simple allosteric model for membrane pumps. Nature. 1966; 211:969–970. [PubMed: 5968307]
14. Vidaver GA. Inhibition of parallel flux and augmentation of counter flux shown by transport models not involving a mobile carrier. J Theor Biol. 1966; 10:301–306. [PubMed: 5964395]
15. Patlak CS. Contributions to the theory of active transport: II. The gate type non-carrier mechanism and generalizations concerning tracer flow, efficiency, and measurement of energy expenditure. Bull. Math. Biophys. 1957; 19:209–235.
16. Krishnamurthy H, Gouaux E. X-ray structures of LeuT in substrate-free outward-open and apo inward-open states. Nature. 2012; 481:469–474. [PubMed: 22230955]
17. Shimamura T, et al. Molecular basis of alternating access membrane transport by the sodium-hydantoin transporter Mhp1. Science. 2010; 328:470–473. [PubMed: 20413494]
18. Watanabe A, et al. The mechanism of sodium and substrate release from the binding pocket of vSGLT. Nature. 2010; 468:988–991. [PubMed: 21131949]
19. Perez C, Koshy C, Yildiz O, Ziegler C. Alternating-access mechanism in conformationally asymmetric trimers of the betaine transporter BetP. Nature. 2012; 490:126–130. [PubMed: 22940865]
20. Shaffer PL, Goehring A, Shankaranarayanan A, Gouaux E. Structure and mechanism of a Na+-independent amino acid transporter. Science. 2009; 325:1010–1014. [PubMed: 19608859]

21. Shi L, Quick M, Zhao Y, Weinstein H, Javitch JA. The mechanism of a neurotransmitter:sodium symporter--inward release of Na+ and substrate is triggered by substrate in a second binding site. Mol Cell. 2008; 30:667–677. [PubMed: 18570870]
22. Shi L, Weinstein H. Conformational rearrangements to the intracellular open states of the LeuT and ApcT transporters are modulated by common mechanisms. Biophys J. 2010; 99:L103–L105. [PubMed: 21156121]
23. Forrest LR, Rudnick G. The rocking bundle: a mechanism for ion-coupled solute flux by symmetrical transporters. Physiology (Bethesda). 2009; 24:377–386. [PubMed: 19996368]
24. McHaourab HS, Steed PR, Kazmier K. Toward the fourth dimension of membrane protein structure: insight into dynamics from spin-labeling EPR spectroscopy. Structure. 2011; 19:1549–1561. [PubMed: 22078555]
25. Freed DM, Horanyi PS, Wiener MC, Cafiso DS. Conformational exchange in a membrane transport protein is altered in protein crystals. Biophys J. 2010; 99:1604–1610. [PubMed: 20816073]
26. Cross TA, Sharma M, Yi M, Zhou HX. Influence of solubilizing environments on membrane protein structures. Trends Biochem Sci. 2011; 36:117–125. [PubMed: 20724162]
27. Hubbell WL, McHaourab HS, Altenbach C, Lietzow MA. Watching proteins move using site-directed spin labeling. Structure. 1996; 4:779–783. [PubMed: 8805569]
28. Jeschke G, Polyhach Y. Distance measurements on spin-labelled biomacromolecules by pulsed electron paramagnetic resonance. Phys Chem Chem Phys. 2007; 9:1895–1910. [PubMed: 17431518]
29. Zhao Y, et al. Single-molecule dynamics of gating in a neurotransmitter transporter homologue. Nature. 2010; 465:188–193. [PubMed: 20463731]
30. Claxton DP, et al. Ion/substrate-dependent conformational dynamics of a bacterial homolog of neurotransmitter:sodium symporters. Nat Struct Mol Biol. 2010; 17:822–829. [PubMed: 20562855]
31. Kniazeff J, et al. An intracellular interaction network regulates conformational transitions in the dopamine transporter. J Biol Chem. 2008; 283:17691–1701. [PubMed: 18426798]
32. Georgieva ER, Borbat PP, Ginter C, Freed JH, Boudker O. Conformational ensemble of the sodium-coupled aspartate transporter. Nat Struct Mol Biol. 2013; 20:215–221. [PubMed: 23334289]
33. Hanelt I, Wunnicke D, Bordignon E, Steinhoff HJ, Slotboom DJ. Conformational heterogeneity of the aspartate transporter Glt(Ph). Nat Struct Mol Biol. 2013; 20:210–24. [PubMed: 23334291]
34. Polyhach Y, Bordignon E, Jeschke G. Rotamer libraries of spin labelled cysteines for protein studies. Phys Chem Chem Phys. 2011; 13:2356–2366. [PubMed: 21116569]
35. Polyhach Y, Godt A, Bauer C, Jeschke G. Spin pair geometry revealed by high-field DEER in the presence of conformational distributions. J Magn Reson. 2007; 185:118–129. [PubMed: 17188008]
36. Quick M, et al. Binding of an octylglucoside detergent molecule in the second substrate (S2) site of LeuT establishes an inhibitor-bound conformation. Proc Natl Acad Sci U S A. 2009; 106:5563–5568. [PubMed: 19307590]
37. Islam SM, Stein RA, McHaourab HS, Roux B. Structural refinement from restrained-ensemble simulations based on EPR/DEER data: application to T4 lysozyme. J Phys Chem B. 2013; 117:4740–4754. [PubMed: 23510103]
38. Roux B, Islam SM. Restrained-ensemble molecular dynamics simulations based on distance histograms from double electron-electron resonance spectroscopy. J Phys Chem B. 2013; 117:4733–4739. [PubMed: 23510121]
39. Zhao Y, et al. Substrate-modulated gating dynamics in a Na+-coupled neurotransmitter transporter homologue. Nature. 2011; 474:109–113. [PubMed: 21516104]

Methods References

40. Quick M, Javitch JA. Monitoring the function of membrane transport proteins in detergent-solubilized form. Proc Natl Acad Sci U S A. 2007; 104:3603–8. [PubMed: 17360689]

41. Pannier M, Veit S, Godt A, Jeschke G, Spiess HW. Dead-time free measurement of dipole-dipole interactions between electron spins. Journal of Magnetic Resonance. 2000; 142:331–40. [PubMed: 10648151]
42. Jeschke G. DEER distance measurements on proteins. Annu Rev Phys Chem. 2012; 63:419–46. [PubMed: 22404592]
43. Jeschke G, et al. DeerAnalysis2006—a comprehensive software package for analyzing pulsed ELDOR data. Applied Magnetic Resonance. 2006; 30:473–498.
44. Chiang YW, Borbat PP, Freed JH. The determination of pair distance distributions by pulsed ESR using Tikhonov regularization. Journal of Magnetic Resonance. 2005; 172:279–95. [PubMed: 15649755]
45. Brooks BR, et al. CHARMM: The Biomolecular Simulation Program. Journal of Computational Chemistry. 2009; 30:1545–1614. [PubMed: 19444816]
46. MacKerell AD, et al. All-atom empirical potential for molecular modeling and dynamics studies of proteins. Journal of Physical Chemistry B. 1998; 102:3586–3616.
47. Mackerell AD, Feig M, Brooks CL. Extending the treatment of backbone energetics in protein force fields: Limitations of gas-phase quantum mechanics in reproducing protein conformational distributions in molecular dynamics simulations. Journal of Computational Chemistry. 2004; 25:1400–1415. [PubMed: 15185334]
48. Lazaridis T. Effective energy function for proteins in lipid membranes. Proteins. 2003; 52:176–192. [PubMed: 12833542]
49. Lazaridis T, Karplus M. Effective energy function for proteins in solution. Proteins. 1999; 35:133–152. [PubMed: 10223287]
50. Jo S, Kim T, Iyer VG, Im W. CHARMM-GUI: a web-based graphical user interface for CHARMM. Journal of Computational Chemistry. 2008; 29:1859–65. [PubMed: 18351591]
51. Adelman SA, Doll JD. Generalized Langevin Equation Approach for Atom-Solid-Surface Scattering - General Formulation for Classical Scattering Off Harmonic Solids. Journal of Chemical Physics. 1976; 64:2375–2388.

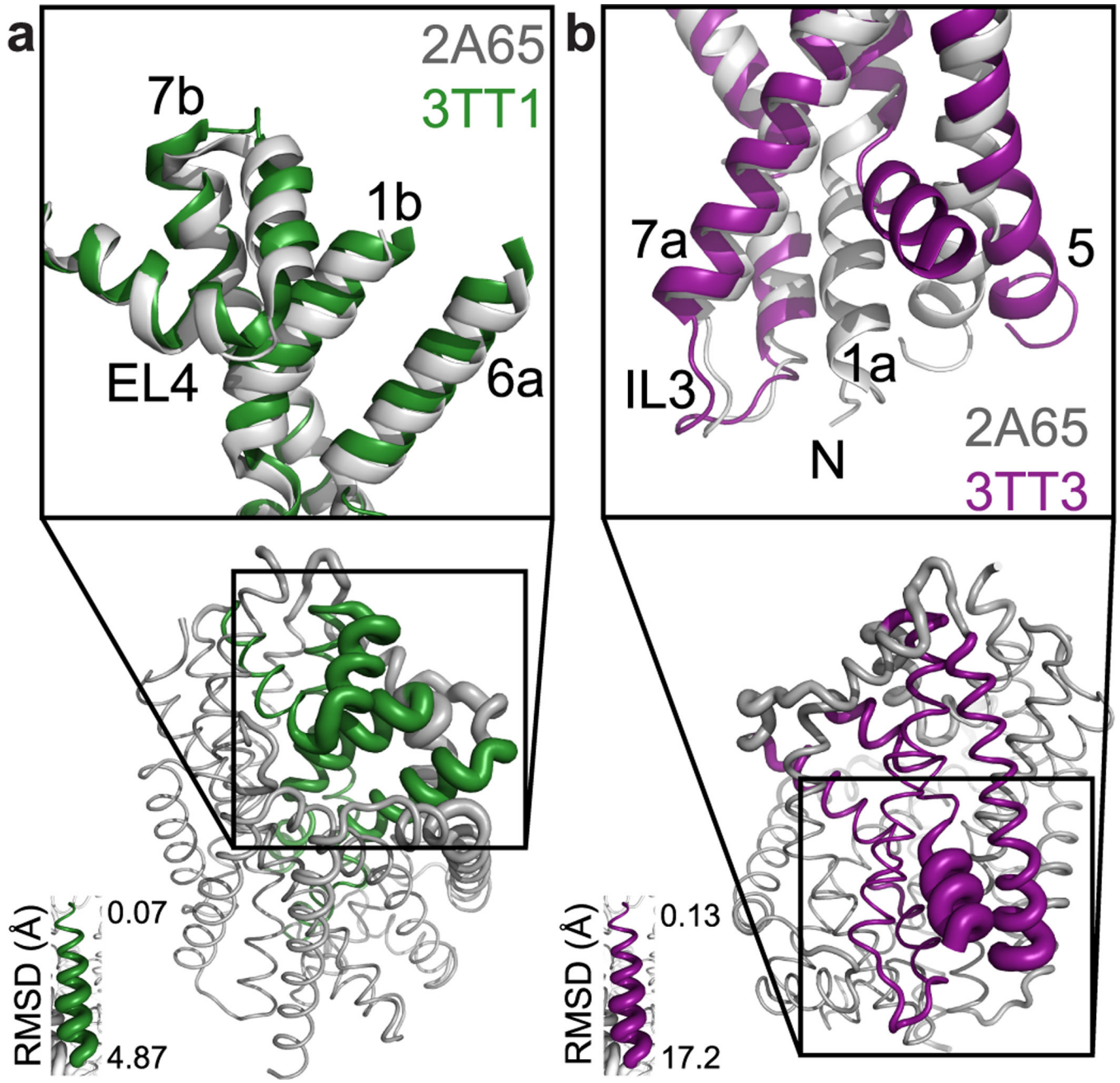

Figure 1. Model of LeuT alternating access inferred from the crystal structures

(**a**) Root mean square deviation (RMSD) between occluded (PDB ID: 2A65)[6] and outward-open (PDB ID: 3TT1)[16] LeuT crystal structures mapped onto the outward-facing substrate-occluded structure. The inset is a close-up view to highlight regions of most substantial differences, TMs 1, 6, and EL4, as well as TM7. (**b**) RMSD between occluded (PDB ID: 2A65) and inward-open (PDB ID: 3TT3)[16] LeuT crystal structures mapped onto a ribbon diagram of the outward-facing substrate-occluded structure. The regions of most appreciable differences (TMs 1 and 5) as well as TMs 6 and 7 are shown in a close up view.

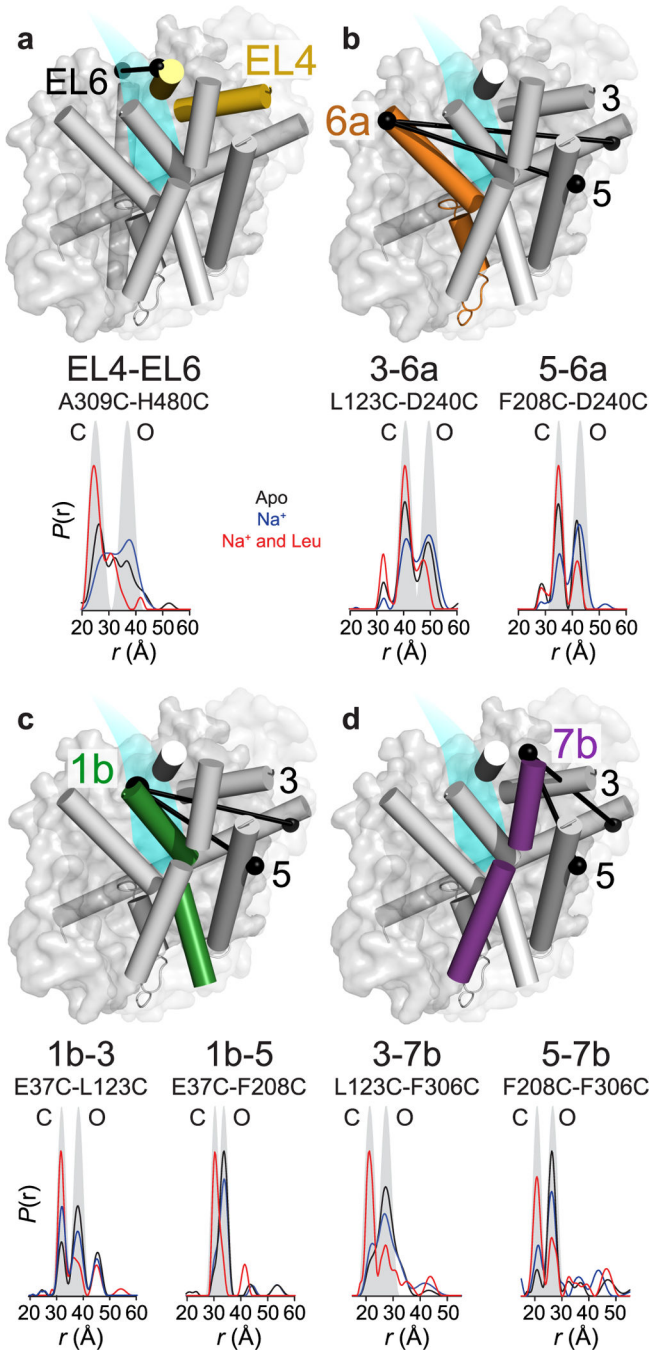

Figure 2. Na^+-induced opening and Na^+- and Leu-induced closing of the LeuT extracellular side

(**a**–**d**) Distance distributions, depicting the probability of a distance P(r) versus distance (r) between spin labels, and reporting the conformational dynamics of EL4, TM6, TM1, and TM7 on the extracellular side of LeuT. The locations of representative spin label pairs are highlighted on the substrate-occluded structure by black spheres connected by a line. TM helices expected to respond to ligand binding are shown as colored cylinders. The approximate location of the extracellular vestibule is colored cyan. Distance distributions for each pair were obtained in the apo, Na^+-bound (Na^+), and Na^+- and Leu-bound (Na^+ and

Leu) intermediates. The multi-component distributions reflect multiple conformations of LeuT in equilibrium. For illustration, we simulated the distance components corresponding to the outward-open (O) and outward-closed (C) conformations using the average distance and width of each component. The resulting Gaussians are superimposed in gray. The shift in the conformational equilibrium of EL4, TM6a, TM1b and TM7b relative to static reference points are shown in **a, b, c**, and **d** respectively.

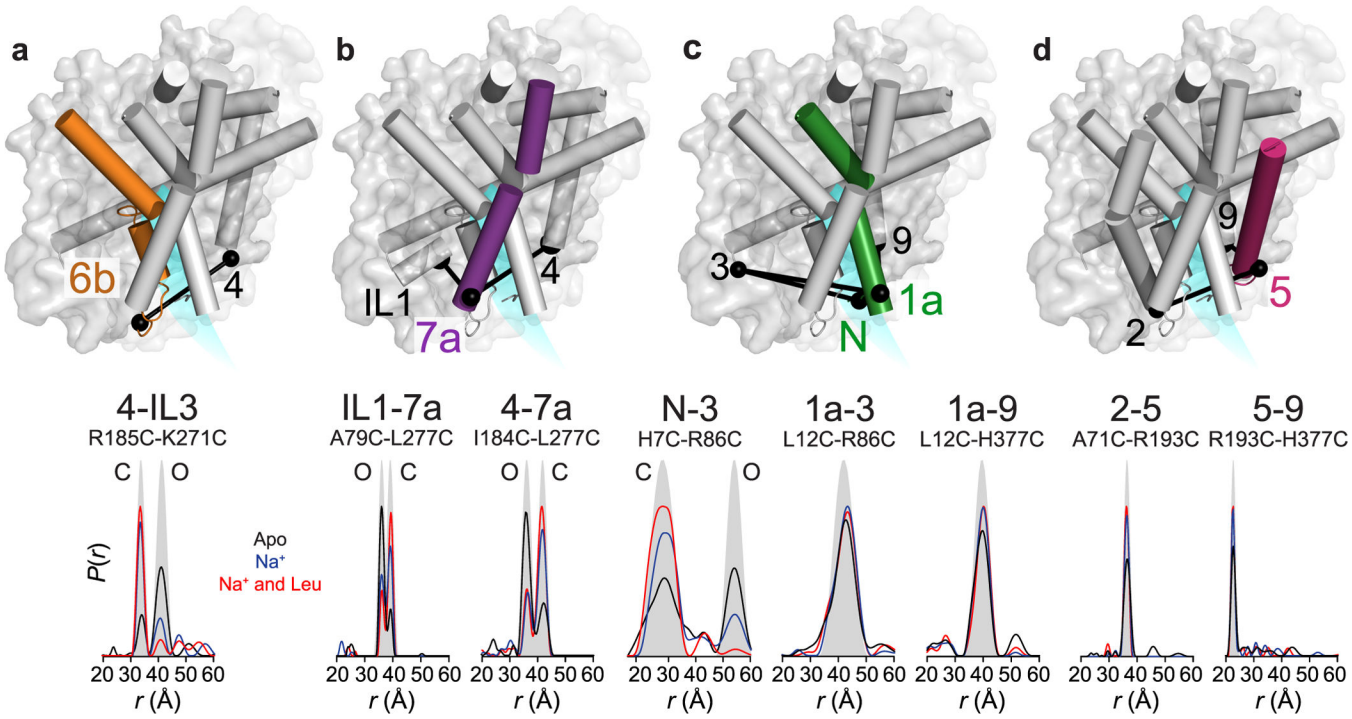

Figure 3. Fluctuation dynamics of TMs 6, 7 and the N-terminal segment mediate the opening of the intracellular side of LeuT

(**a**–**d**) Distance distributions, depicting the probability of a distance P(r) versus distance (r) between spin labels, and reporting the conformational dynamics of IL3, TM7, TM1, and TM5 on the intracellular side of LeuT. Distance distributions for each pair were obtained under three conditions as in Figure. 2. Here, the simulated grey distributions reflect inward-open (O) and inward-closed (C) conformations. (**a,b**) TM7 and IL3 distributions indicate an equilibrium between two conformations that is modulated by Na^+ and substrate binding. (**c,d**) In contrast, distributions for TMs 1 and 5 do not indicate ligand-dependent conformational changes.

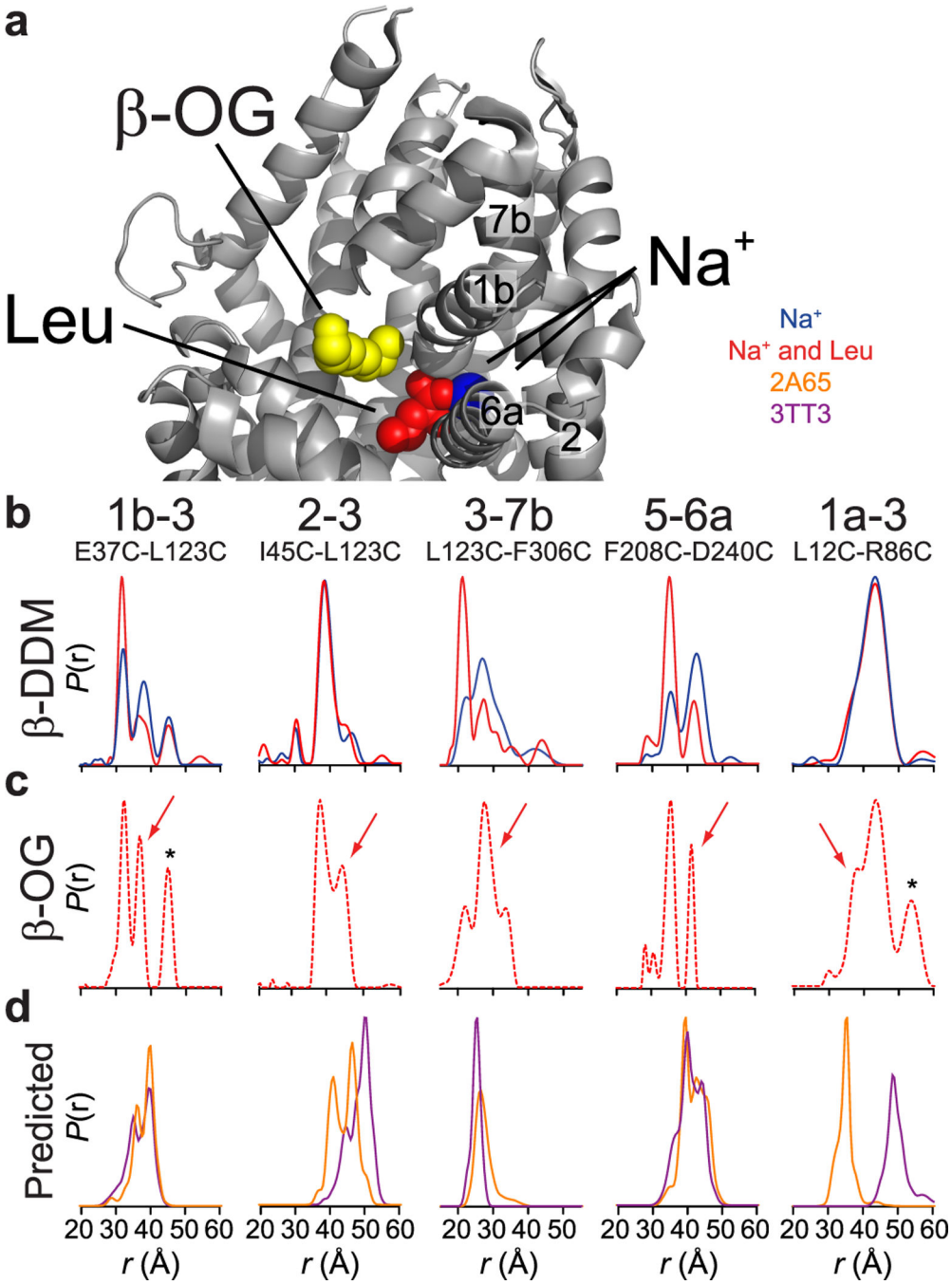

Figure 4. β-OG stabilizes the outward-facing conformation of LeuT in the presence of Na^+ and leucine

(**a**) Close-up view of LeuT extracellular vestibule showing the simultaneous binding of leucine (red), Na^+ (blue) and β-OG (yellow) (PDB ID: 3GJD). Comparison of distance distributions in β-DDM (**b**) and β-OG (**c**) demonstrate that the latter stabilizes an outward-facing conformation on the extracellular side and a closed conformation on the intracellular side (TM1a and 3). The corresponding distance component is indicated by an arrow. The component labeled * arises from aggregated protein during the concentration process. (**d**)

Predicted distance distributions from three LeuT crystal structures (3TT1: outward-facing, 2A65: substrate-occluded, 3TT3: inward-facing) using MMM (see methods).

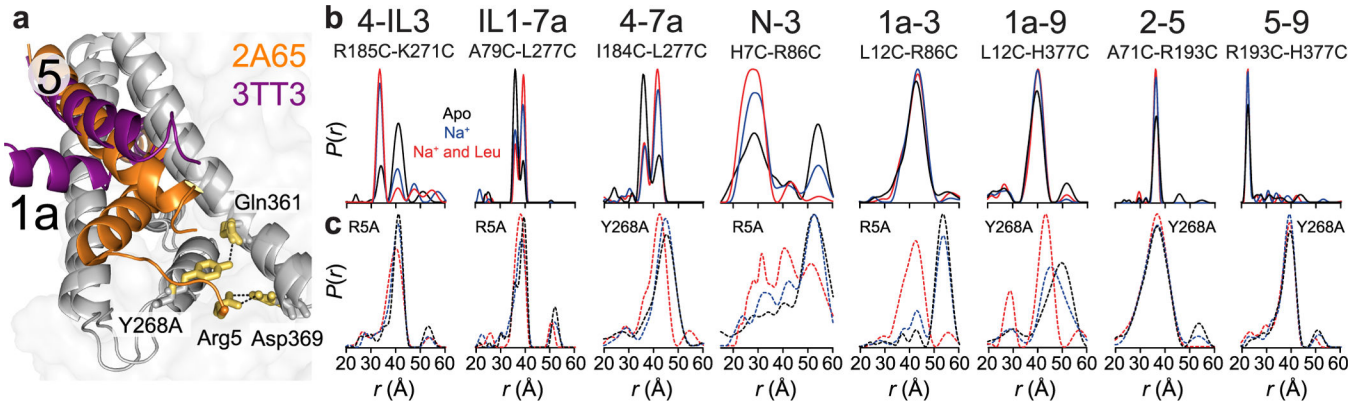

Figure 5. The Y268A or R5A mutations induce structural rearrangements in LeuT

(**a**) Close up view of the putative intracellular gate showing the network of charge interactions stabilized by Tyr268 and involving Arg5. TMs 1 and 5, are highlighted. (**b,c**) the mutations Y268A and R5A lead to the appearance of new distance components in the distributions of TMs 1 and 5 (dashed lines, **c**) that is not present in the WT background (**b**) under apo conditions.

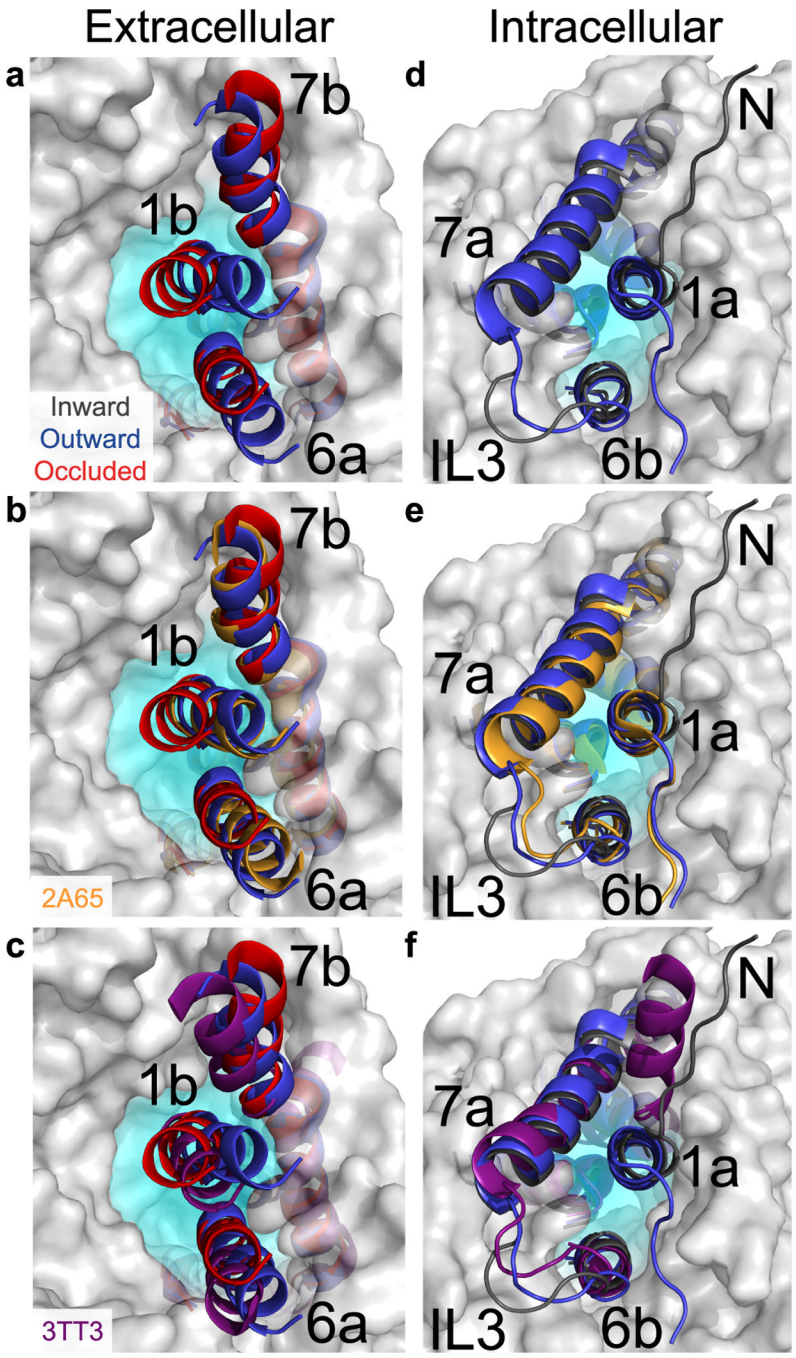

Figure 6. Models of LeuT conformational changes derived from restrained ensemble simulations

(**a**–**c**) Extracellular view of the occluded (red) and outward-facing (blue) models of LeuT, derived from the DEER restraints, superimposed on (**b**) the substrate-occluded crystal structure (2A65, orange) and (**c**) the inward-facing crystal structure (3TT3, purple). Prominent displacements of TMs 1 and 6 (red model) to close the extracellular vestibule are observed in the occluded conformation relative to the crystal structures. (**d**–**f**) Intracellular view of the inward-facing model (black), derived from the DEER restraints, superimposed

on (**d**) the outward-facing model (blue), (**e**) the substrate-occluded structure (2A65, orange) and (**f**) the inward-facing structure (3TT3, purple).

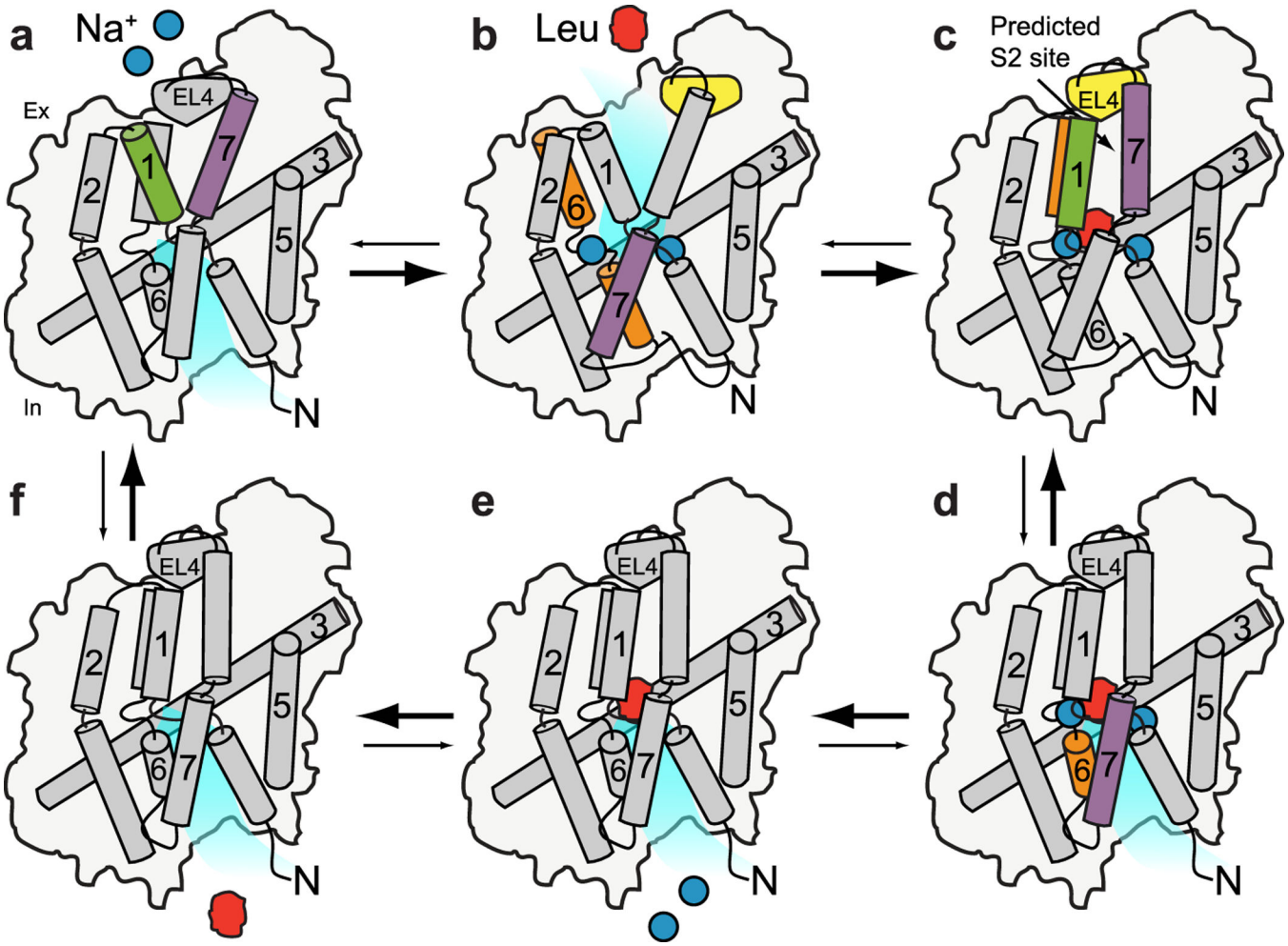

Figure 7. Cartoon model of LeuT transport derived from EPR data

Transmembrane helices involved in conformational changes at each step in the transport cycle are highlighted in color. (**a**) The cycle begins following release of ion and substrate to the intracellular side (In). Apo-LeuT samples inward- (**a**) and outward-facing conformations (**b**). (**b**) Na^+ binding favors opening of the extracellular side (Ex) through shifts in the equilibrium of the extracellular motifs. Coupled closing of the intracellular side involves a shift in the equilibrium of the intracellular motif to its closed position, which stabilizes the intracellular gate. (**c**) Leu binding at the S1 site, and presumably at the S2 site as well, causes a large scale closure of the extracellular side leading to an occluded state. (**d**) Fluctuations on the intracellular side, facilitated by the unwound region of TM6 and a kink at Gly294 of TM7 mediate the opening of the intracellular side. (**e**) Na^+ dissociates to the intracellular solution where its concentration is low. (**f**) In the absence of bound Na^+, leucine affinity to LeuT is reduced driving its dissociation to the intracellular side. The cycle continues through the isomerization from inward-facing (**f**) to outward-facing (**a**).